

Pouring time into space

Jan F.G. Schneiders¹, Iliass Azijli¹, Fulvio Scarano¹ and Richard P. Dwight¹

¹ Department of Aerospace Engineering, TU Delft, Delft, The Netherlands
J.F.G.Schneiders@tudelft.nl

A method is proposed to reconstruct instantaneous velocity from time-resolved tomographic PTV, employing both instantaneous velocity and velocity material derivative. This improves upon current techniques by not only including penalization of velocity divergence, but also requiring consistency with the temporal derivative of the PTV particle tracks. Hence the procedure is christened as *pouring time into space*. The aim of the proposed technique is to increase spatial resolution of tomographic PTV in cases where it is limited by the seeding concentration. An inverse problem is solved to find the velocity field that minimizes a cost function including next to instantaneous velocity and its divergence, also the velocity material derivative. The velocity and its material derivative are related through the vorticity transport equation and the problem is minimized using the L-BFGS algorithm, where gradients are evaluated efficiently using an adjoint implementation of the method. The procedure is assessed numerically using results from a simulated PTV experiment in a turbulent boundary layer from DNS, and experimentally using tomographic PIV measurements in a jet flow. Both the numerical and experimental assessment show that the proposed technique yields improved accuracy of the velocity field in between the measured points over penalization of divergence only, thereby demonstrating that the temporal information available in time-resolved tomographic PTV can be leveraged to increase reconstruction quality of instantaneous velocity.

1 INTRODUCTION

For both tomographic PIV and PTV measurements, the achievable spatial resolution is related to the tracer particle concentration, as for tomographic PIV interrogation volumes containing approximately 5 particles are typically used and for PTV scattered velocity measurements are available at particle locations only. Maximum seeding concentration and thereby spatial resolution is typically dictated by the maximum particles per pixel (ppp) that can be dealt with by the tomographic reconstruction in view of the ghost particles phenomenon (Elsinga et al. 2006; Lynch and Scarano 2015). For experiments in water, an additional constraint is imposed by opacity and multiple scattering. Increasing measurement volume size reduces the maximum seeding concentration and spatial resolution for tomographic measurements in both air and water. Also, recent efforts towards large-scale PIV using Helium-filled soap bubbles (HFSB) as tracers report that spatial resolution is mostly limited by the production rate of the HFSB (Scarano et al 2015).

Avoiding the interrogation volume size dependent filtering effect of tomographic PIV, particle tracking techniques promise an increase in spatial resolution. Stitou and Riethmuller (2001) discussed further the possibility of super-resolution PIV originally introduced by Keane et al (1995), by refining the PIV result using a PTV algorithm. In the case of time-resolved tomographic PTV, the particle trajectories can be leveraged to increase accuracy of the velocity measurements (Malik 1993) and for accurate volume reconstruction and particle tracking at high levels of source density (viz. ppp) on the order of tomographic PIV (shake-the-box, Schanz et al. 2013). The resulting velocity measurements are available at the scattered instantaneous particle positions. To allow for data post-processing and visualization using codes requiring data on a uniform grid, the trivial approach to reconstruct the measurements on a uniform grid is tri-linear interpolation (Figure 1, left) or averaging velocity vectors in an interrogation window analogously to PIV (Figure 1, middle). Alternatively, post-processing methods can be rewritten to handle data on scattered grids, as proposed for example by Neeteson and Rival (2015) for solution of the pressure-Poisson equation.

More advanced techniques reconstruct a filtered velocity field on a uniform grid from the scattered measurement data. Such techniques have been widely addressed in literature and examples include adaptive Gaussian windowing (AGW, introduced by Agüí and Jiménez, 1987) and radial basis function interpolation (RBF, amongst others Casa and Krueger, 2013). This comes however at the cost of low-pass filtering the result, reducing again spatial resolution. The regularization and spatial resolution of the result can potentially be improved by invoking the incompressibility constraint. Zhong et al. (1991)

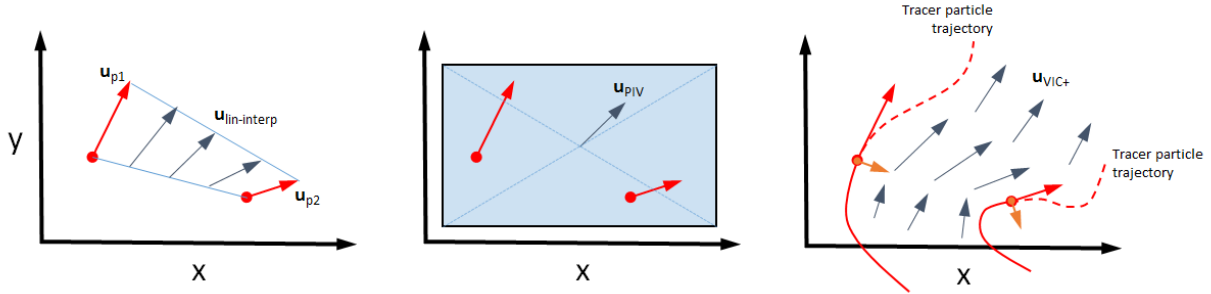


Figure 1 Velocity reconstruction techniques; from left: linear interpolation between two PTV velocity measurements, middle: PIV interrogation window approach and right: VIC+ interpolation between two PTV particle trajectories.

Vedula and Adrian (2005) and Azijli et al (2014) impose a regularization term such that the reconstructed velocity field is analytically divergence free. Also the recently proposed shake-the-box method (Schanz et al. 2013) includes divergence free penalization in a B-spline based regularization technique allowing for manual weighting of the incompressibility constraint. It should be remarked that techniques invoking the incompressibility constraint are applicable to volumetric measurements only, as from planar PIV no information on the out-of-plane velocity gradient is available and the in-plane velocity field is rarely divergence free in applications involving turbulent flow fields.

For PIV measurements where not spatial but temporal resolution is insufficient (i.e. below Nyquist), Scarano and Moore (2012) have proposed a technique that leverages information available by instantaneous velocity measurements in the spatial domain to increase resolution in the temporal domain. Using a linearized advection equation the technique reconstructs the velocity temporal evolution in between temporally under-sampled measurements. This procedure was christened “*pouring space into time.*” It was demonstrated to reconstruct past the Nyquist limit in flows where the assumption of frozen turbulence holds. Later the concept was generalized by Schneiders et al. (2014) to general incompressible flow cases by extending the linearized advection equation to the vorticity transport equation using the vortex-in-cell (VIC) technique for three-dimensional measurements as issued by tomographic PIV.

Analogously, information in the temporal domain has been employed recently for increased accuracy of measurements in the spatial domain. The FTC (Lynch and Scarano, 2013) and FTEE (Jeon et al, 2014) techniques have demonstrated improved correlation for time-resolved tomographic PIV and the MTE (Novara and Scarano, 2010). Shake-the-box (Schanz et al. 2013) and SMTE (Lynch and Scarano, 2015) show improved reconstruction of particle volumes from time-resolved tomographic measurements. The use of additional flow physics for reconstruction of velocity from time-resolved PIV images has received attention also in the field of optical flow, where in recent studies the vorticity transport equation is leveraged with a variational reconstruction technique, as discussed in the review paper by Heitz et al. (2010).

These techniques have not yet dealt with increasing spatial resolution of the instantaneous velocity measurements, in cases where the spatial resolution is limited by tracer particle seeding concentration. However, as information in the spatial domain has proven to allow for an increase in temporal resolution, potentially the reverse can allow for an increase in spatial resolution. This reversed principle is therefore christened as *pouring time into space.* The spatial and temporal information is linked through the flow governing equations, i.e. Navier-Stokes. In contrast to invoking only the incompressibility constraint, this yields a non-linear system of equations and making the reconstruction problem a non-linear optimization problem. To avoid the window-size dependent filtering effect of tomographic PIV, tomographic PTV measurements are considered here. Time-resolved tomographic PTV measures the displacement of individual tracer particles and the temporal information is available in the form of Lagrangian trajectories of the tracer particles (Figure 1, right); i.e. velocity \mathbf{u}_m is measured at particle locations \mathbf{x}_p at each measurement time-instant t_i . In a variational framework, the velocity reconstruction \mathbf{u}_h on a computational grid with node-spacing h becomes the solution of a minimization problem with cost function,

$$(1) \quad J = \sum_{i=1}^{N_t} \sum_{p=1}^{N_p} [\mathbf{u}_h(\mathbf{x}_p(t_i), t_i) - \mathbf{u}_m(\mathbf{x}_p(t_i), t_i)]^2 + \beta \sum_{i=1}^{N_t} \|\nabla \cdot \mathbf{u}_h(\mathbf{x}, t_i)\|,$$

where \mathbf{u}_h is the reconstructed velocity field, N_t the number of measurement time-instants, N_p the number of particles in the measurement volume and β a coefficient weighting the divergence free constraint. Considering the computational cost of an iterative minimization procedure solving at each time-instant a solution of the flow governing equations, a simplified method can be envisaged by introducing the temporal information through the velocity material derivative,

$$(2) \quad J = \underbrace{\sum_{p=1}^{N_p} [\mathbf{u}_h(\mathbf{x}_p(t_1), t_1) - \mathbf{u}_m(\mathbf{x}_p(t_1), t_1)]^2}_{\text{divergence free regression}} + \beta \sum \|\nabla \cdot \mathbf{u}(\mathbf{x}, t_i)\| + \alpha \underbrace{\sum_{p=1}^{N_p} \left[\frac{D\mathbf{u}_h}{Dt}(\mathbf{x}_p(t_1), t_1) - \frac{D\mathbf{u}_m}{Dt}(\mathbf{x}_p(t_1), t_1) \right]^2}_{\text{temporal information}}.$$

The first two terms in this optimization involve the instantaneous velocity measurements and the incompressibility constraint as done in previous works cited before (e.g. ‘‘flow-fit’’ Schroder et al. 2015). The additional third term in the cost function introduces temporal information in form of the velocity material derivative available by tomographic PTV to the reconstruction of instantaneous velocity.

The goal of the present study is to determine whether the constraint imposed by this additional term allows for an increase in reconstruction accuracy of velocity on a uniform grid. In other words, whether the temporal information can be leveraged and ‘poured into the spatial domain’ when reconstructing velocity on a grid from time-resolved tomographic PTV measurements. In the next section it is outlined how the problem is solved efficiently with gradient-based optimization and an adjoint of the method. Subsequently, sections 3 and 4 consider respectively numerical and experimental assessment of the method.

2 THE VIC+ METHOD

Consider a time-resolved PTV measurement volume Ω with boundary $\partial\Omega$. The proposed velocity reconstruction technique aims to find the degrees of freedom,

$$(3) \quad \xi = \{\xi_\omega, \xi_u, \xi_{\partial u}\} = \left\{ \omega|_\Omega, c_1 \mathbf{u}|_{\partial\Omega}, c_2 \frac{\partial \mathbf{u}}{\partial t}|_{\partial\Omega} \right\},$$

that minimize the cost function

$$(4) \quad J = J_u + J_{Du} + J_r = \underbrace{\sum_p \|\mathbf{u}_h(\mathbf{x}_p) - \mathbf{u}_m(\mathbf{x}_p)\|^2}_{J_u} + \alpha \underbrace{\sum_p \left\| \frac{D\mathbf{u}_h}{Dt}(\mathbf{x}_p) - \frac{D\mathbf{u}_m}{Dt}(\mathbf{x}_p) \right\|^2}_{J_{Du}} + \underbrace{\beta_1 \sum \|\nabla \cdot \omega\|^2 + \beta_2 \sum \|\nabla \cdot \mathbf{u}\|^2}_{J_r}.$$

The degrees of freedom (3) consist of vorticity within the measurement volume and velocity and its temporal derivative on the boundary. The coefficients c_1 and c_2 in (3) define the relative scaling of the degrees of freedom. In the present study they are set such that the RMS of the adjoint of each of the separate components is of the same order of magnitude, to avoid optimization of one component of (3) only. The cost function consists of J_u for the instantaneous velocity measurement, J_{Du} for the instantaneous velocity material derivative measurement and J_r for penalization of velocity and vorticity divergence. The coefficients α , β_1 and β_2 make the cost function dimensionally consistent and allow for relative scaling of the different components (see section 2.2 for details on setting their values).

The minimization is performed using the gradient-based limited-memory BFGS method (Liu and Nocedal, 1989), where the gradients $\partial J / \partial \xi$ are evaluated using an adjoint implementation of the method. The iterative optimization procedure starts from an initial guess of the degrees of freedom (3) on the computational uniform grid with node-spacing h . To enforce a connection between the grid values of vorticity, the vorticity field is discretized on the grid using Gaussian radial basis functions with standard deviation equal to the mesh spacing h . The initial guess of ξ can follow from for example PIV analysis or one of the PTV velocity reconstruction techniques mentioned in the introduction. For reconstruction of subsequent time-instants, time supersampling (Schneiders et al. 2014) can be applied to approximate the velocity field and initial condition at that time-instant. The method is christened VIC+, as it is inspired by time-supersampling using VIC simulation (Schneiders et al. 2014) ‘plus’ the use of PTV particle track information. A flowchart of the method is given in Figure 2. The computation steps are explained in more detail in the next section. In section 2.2 it is discussed how the coefficients α , β_1 and β_2 and mesh spacing h are determined.

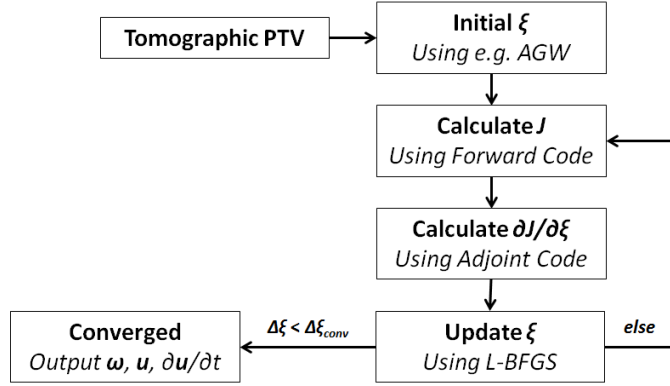


Figure 2 Flowchart of the proposed method

2.1 Forward code

The forward code calculates at each iteration the cost function (4) in three steps:

Step 1: Calculation of J_u

Velocity is calculated on a uniform grid with node-spacing h by solution of a Poisson equation,

$$(5) \quad \nabla^2 \mathbf{u} = -\nabla \times \boldsymbol{\omega},$$

with boundary conditions on velocity provided by (2). Second-order central differences are used for evaluation of all the spatial derivatives, except at the volume boundaries where first-order single-sided differences are used. Subsequently, velocity is interpolated to the particle locations using linear interpolation, allowing direct calculation of J_u .

Step 2: Calculation of J_{Du}

The convective term of the velocity material derivative

$$(6) \quad \frac{D\mathbf{u}}{Dt} = \frac{\partial \mathbf{u}}{\partial t} + (\mathbf{u} \cdot \nabla) \mathbf{u},$$

can be readily calculated from the velocity field calculated on the uniform grid in step 1. To approximate the temporal derivative of velocity, first the temporal vorticity derivative is calculated from the vorticity transport equation,

$$(7) \quad \frac{\partial \boldsymbol{\omega}}{\partial t} = (\boldsymbol{\omega} \cdot \nabla) \mathbf{u} - (\mathbf{u} \cdot \nabla) \boldsymbol{\omega}.$$

The temporal velocity derivative is subsequently calculated by solving a second Poisson equation,

$$(8) \quad \nabla^2 \frac{\partial \mathbf{u}}{\partial t} = -\nabla \times \frac{\partial \boldsymbol{\omega}}{\partial t},$$

with boundary conditions on $\partial \mathbf{u} / \partial t$ from $\boldsymbol{\xi}_{\partial \mathbf{u}}$. The velocity material derivative is subsequently calculated on the grid and interpolated using a linear interpolation to the particle locations, allowing for evaluation of J_{Du} .

Step 3: Calculation of J_r

Divergence of velocity and vorticity are calculated on the full measurement grid using again second order central differences, allowing for direct evaluation of J_r .

2.2 Coefficient determination and a-posteriori reconstruction error estimation

The coefficients α and $\beta_{1,2}$ determine respectively how the L-2 norm of the error in the velocity material derivative and the regularization terms are scaled in the cost function (3). As a rule of thumb, the amount of regularization must scale with the expected noise level in the measurements. More quantitatively, the coefficients α , β_1 and β_2 , and also mesh spacing h , can be tuned to their optimal values by splitting the scattered measurements into three sets: a set used for the velocity reconstruction and a training set and a benchmark set for *a-posteriori* reconstruction error assessment,

$$(9) \quad \varepsilon = \sqrt{\frac{1}{N_{bench}} \sum \|\mathbf{u}(\mathbf{x}_{p bench}) - \mathbf{u}_{m,p bench}\|^2}.$$

The training set is used to tune the coefficients in the procedure, such that the error is minimized. Determination of a general rule for determination of the optimal coefficient values and mesh spacing is left as a topic for further research.

The benchmark set is not used in the procedure and allows for *a-posteriori* approximation of the reconstruction accuracy. Here it is assumed that the benchmark and training particle tracks provide an independent velocity measurement at significantly higher accuracy than the velocity reconstruction. Provided the PTV measurement at relatively low seeding concentration is largely free of ghost particles and considering the particle tracks used for benchmarking are not used in the reconstruction procedure, they can be considered independent and because they are typically obtained from a polynomial fit through the particle positions in a track, their accuracy is considered at least one order of magnitude higher than that of the velocity reconstruction.

3. ASSESSMENT FROM SIMULATED TURBULENT BOUNDARY LAYER

The goal of this numerical assessment is to establish the potential increase in reconstruction accuracy when reconstructing velocity from PTV measurement data using the proposed technique. The measurement volume considers a turbulent boundary layer over a flat plate, simulated from a direct numerical simulation (DNS) by Bernardini and Pirozzoli (2011). This DNS dataset has been used before for assessment of tomographic PIV techniques by Probsting et al (2013) and Lynch and Scarano (2015). The simulated measurement volume ($L_x/\delta_{99} = L_z/\delta_{99} = 3$, $L_y/\delta_{99} = 1$) considers the full boundary layer thickness. Isosurfaces of Q-criterion from the DNS reference are given in Figure 3 and relevant parameters of the turbulent boundary layer are given in Table 1.

Simulated PTV measurement results are made by interpolating instantaneous point values of \mathbf{u} and $D\mathbf{u}/Dt$ to a random

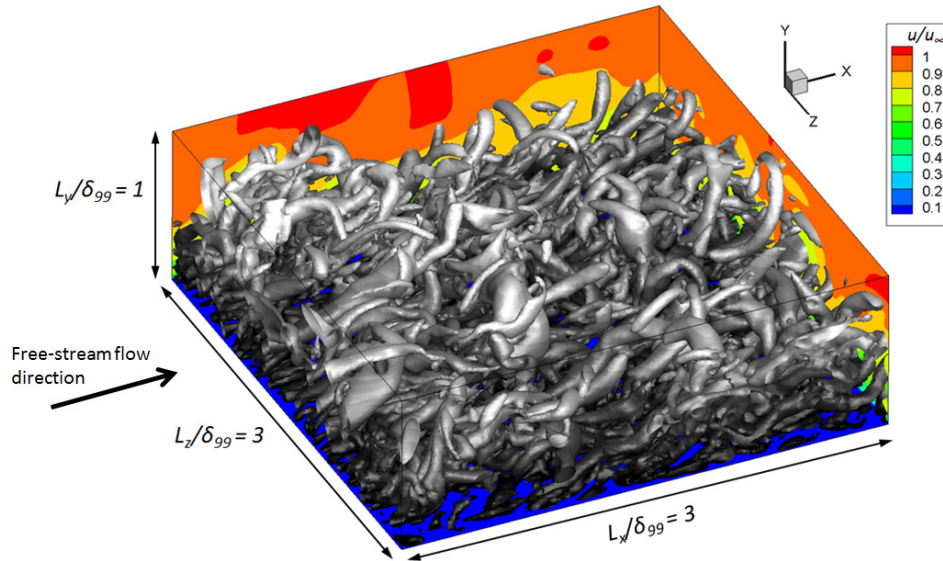
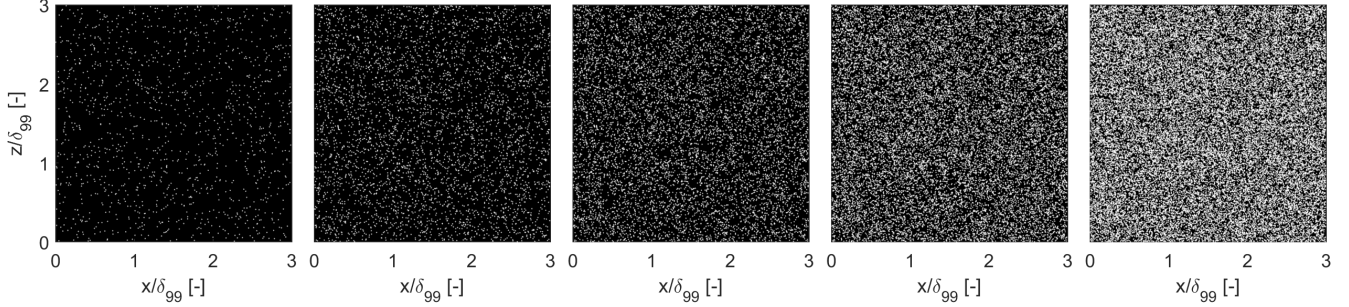


Figure 3 Isosurfaces of Q-criterion in the simulated measurement volume as calculated from the DNS reference.

Table 1 Boundary layer parameters

Displacement thickness	δ^* / δ	0.18
Momentum thickness	θ / δ	0.12
Wall shear velocity	u_τ / u_∞	0.053
Shape factor	H	1.50
Reynolds number	Re_δ	8185
	Re_θ	1000
	Re_τ	325
Timescale ratio	Re_T	23.3

**Figure 4** Particle images of the test cases considered; from left to right $C = 150, 500, 1000, 2000$ and 4000 particles/ δ_{99}^3 .

distribution of particles in the volume. The seeding concentration is constructed to be constant in the measurement volume, and a range of seeding concentrations are considered to assess reconstruction quality at different levels of seeding density. Figure 4 shows simulated particle images at the range of seeding concentrations considered. Considering the focus here is only on assessment of the potential of the proposed method to increase reconstruction accuracy, the measurement results are assumed to be exact and the effect of ghost particles is not considered for conciseness.

Reconstruction of the velocity field on a uniform grid is done using (i) PIV, (ii) trilinear interpolation, (iii) Adaptive Gaussian Window (AGW), (iv) the proposed method using only divergence free penalization (i.e. $\alpha = 0$ and also termed solenoidal filtering) and (v) the proposed method including the velocity material derivative (i.e. VIC+). For PIV, the cross-correlation operator is modeled as a spatial average over an interrogation volume sized such that $\overline{N}_I = 8$. In the present case the interrogation box size is $0.2\delta_{99}$ when the concentration is 1000 particles/ δ_{99}^3 and all particles within the interrogation box are given equal weight. Especially at the lower range of seeding concentrations considered, this PIV approach is expected to introduce strong filtering artifacts. This is confirmed by the isosurfaces of the resulting Q-criterion using the PIV approach plotted in Figure 5b. This figure shows a top-view (along wall-normal direction) of the measurement volume. Because measurement errors are not considered here, a significant improvement is expected already by using the trilinear interpolation through the velocity measurements, as visible over the full range of seeding concentrations considered in Figure 5c. For AGW method the volume size is set such that there is one particle per σ^3 , where σ is the standard deviation of the Gaussian. The method is however still filtering the result and as exact velocity measurements are considered a slight reduction in reconstruction accuracy with respect to Linear interpolation is expected. This is confirmed quantitatively by the L2 errors in Figure 6, showing approximately 10% larger reconstruction errors for AGW in comparison to trilinear interpolation.

Both solenoidal filtering and VIC+ are expected to improve upon the trilinear interpolation as both techniques are incorporating further constraints from a-priori knowledge about the flow physics in the reconstruction. The isosurfaces plotted in Figure 5e and 5f show a significant increase in the level of returned details for both techniques over the full range of seeding concentrations considered. Quantitatively, at $y/\delta_{99} = 0.25$ the rms errors with respect to trilinear interpolation are reduced by 20-30% and 40% for respectively solenoidal filtering and VIC+ (Figure 6).

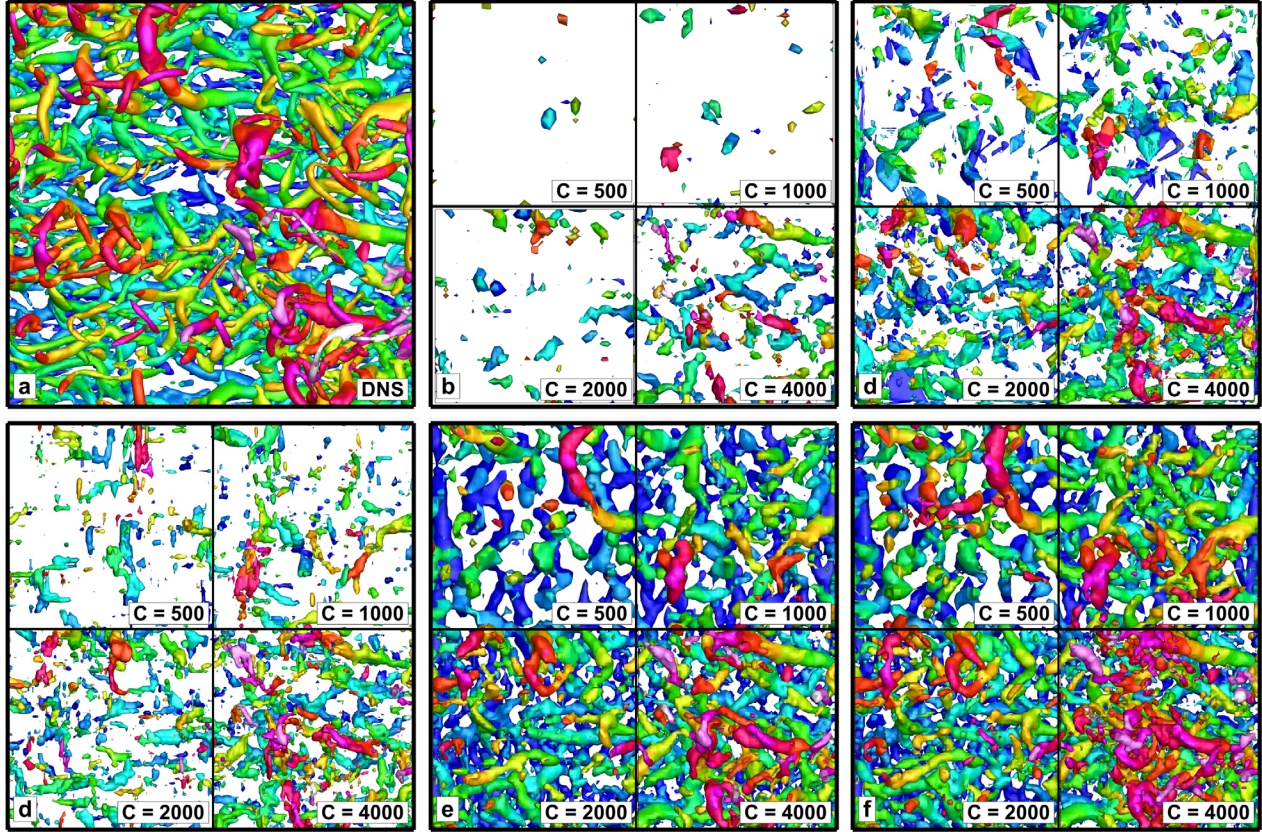


Figure 5 Isosurfaces of Q-Criterion (colored by distance from the wall for clarity) obtained by the different reconstruction methods at a range of seeding concentrations C (in particles/ δ_{99}^3); (a) DNS reference, (b) PIV, (c) Linear interpolation, (d) AGW, (e) divergence free regression, (f) VIC+.

To illustrate how the application of the techniques impacts experimental estimation of relevant flow parameters, consider the turbulent statistics plotted in Figure 7 for the range of seeding concentrations considered. Relatively small differences are expected for u' as this is associated with low and high-speed streaks occurring as rather elongated structures, which correspond to relatively small wavenumbers. In contrast, in the wall-normal velocity fluctuations corresponding to smaller flow structures such hairpins and hairpin packets (e.g. Adrian et al. 2000) are expected to be poorly captured at low

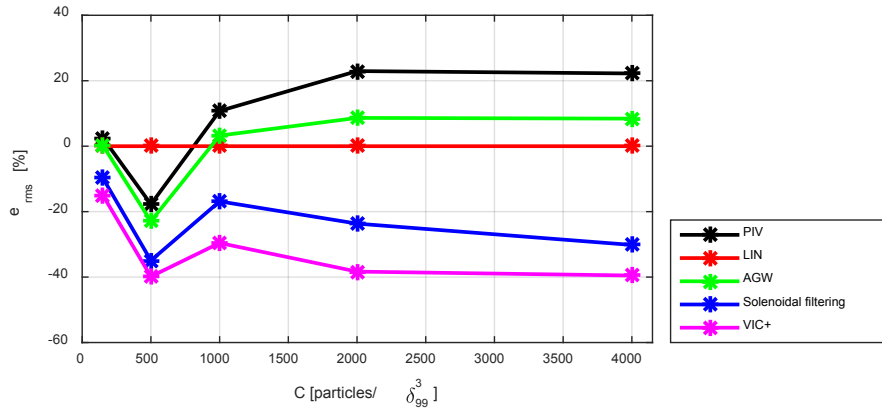


Figure 6 L2 error in the w-component of velocity for the different reconstruction methods, in the plane $y/\delta_{99} = 0.25$ and $x/\delta_{99} = z/\delta_{99} = [0.75, 2.25]$, normalized with respect to linear interpolation.

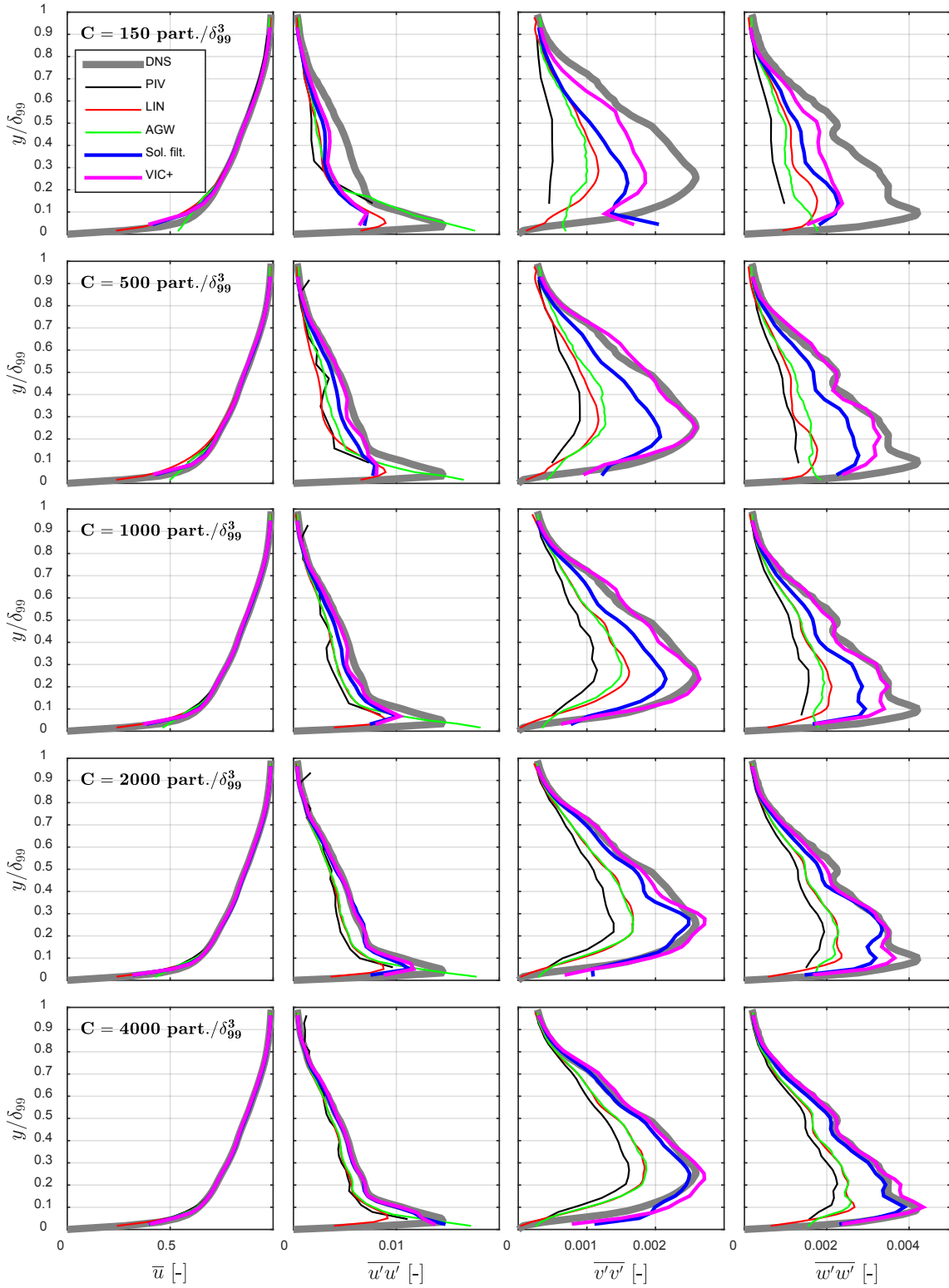


Figure 7 Turbulence statistics calculated from the different velocity field reconstructions; from top to bottom $C = 150, 500, 1000, 2000$ and 4000 particles/ δ_{99}^3 .

concentration of tracers, as their wavenumbers are filtered by the different reconstruction techniques. This is confirmed by the results plotted in Figure 7. For the lowest seeding concentration of 150 particles/ δ_{99}^3 , essentially all methods fail to return an acceptable reconstruction of the turbulent velocity fluctuations, as also indicated by the rms errors in Figure 6. However, already at 500 particles/ δ_{99}^3 , VIC+ is able to reconstruct the correct level of turbulent statistics in the boundary layer for $y/\delta_{99} > 0.2$. Solenoidal filtering requires a seeding concentration more than four times larger before it yields a similar reconstruction and for all seeding concentrations considered, PIV, AGW and trilinear interpolation yield significantly filtered results.

4. EXPERIMENTAL ASSESSMENT

For the experimental assessment, data from an available time-resolved tomographic PIV measurement of a circular jet in water (Fig. 8-left) by Violato and Scarano (2011) is reprocessed using tomo-PTV to obtain particle tracks (Fig. 8-middle). Salient features of the tomographic PIV experiment are given in Table 2 and for further details the reader is referred to Violato and Scarano (2011). For the tomo-PTV procedure, intensity volumes are reconstructed using the MART algorithm and particle volumes are reconstructed using the MART algebraic reconstruction technique (Elsinga et al. 2006). Particles are identified by peak-finding in a 5x5x5 voxel neighbourhood and sub-pixel accuracy of particle location is obtained by fitting of a Gaussian through their intensity distribution. Particle tracks are identified with a length of at least 30 snapshots using a multi-step PTV algorithm based on Malik and Papantoniou (1993). The 3rd order polynomial fit considers 15 consecutive snapshots and yields instantaneous velocity and its material derivative.

A small subset of the full set of tracks is considered to simulate a low seeding concentration ($ppv = 9.1 \times 10^{-7}$, Fig. 8-right). With such coarse distribution of information, the reconstruction of the instantaneous velocity and associated vortices (Q-criterion) using scattered tri-linear interpolation (Fig. 9-left) is not possible. Solenoidal filtering improves upon the linear interpolation (Fig. 9-middle), but is not yet able to reproduce the vortex rings pattern. Including in the minimization the measured velocity material derivative (VIC+) yields in this case a significant addition to the reconstruction of the spatial velocity and vorticity distribution, as the vortex rings are retrieved more clearly (Fig. 9-right).

Table 2 Experimental parameters for the transitional jet following Violato and Scarano (2011)

Jet exit velocity	0.5 m/s
Seeding	Polyamide particles, 56 μm diameter
Illumination	Quantronix <i>Darwin-Duo</i> Nd-YLF laser (2 x 25 mJ @ 1 kHz)
Recording devices	4 x Lavisision <i>HighSpeedStar 6</i> CMOS
Imaging	$f = 105 \text{ mm}$ Nikon objectives
Repetition rate	1,000 Hz
Measurement field	(cylindrical) 30 mm (d) x 50 mm (h)

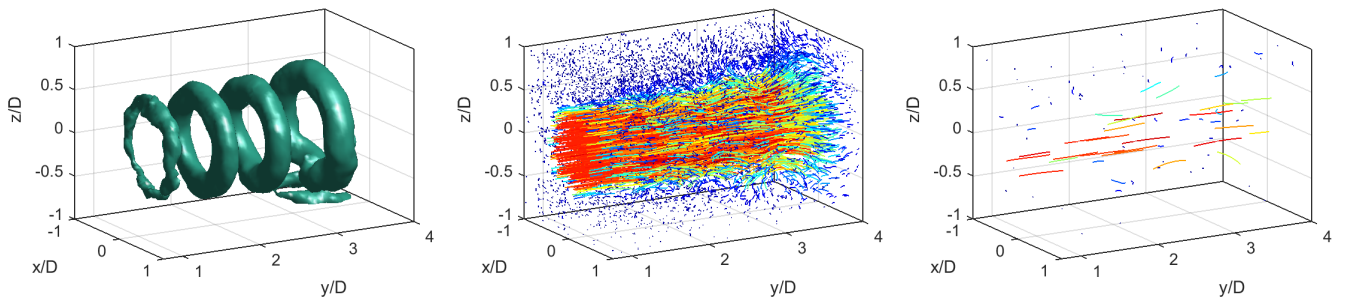


Figure 8 Result from tomo-PIV/PTV measurements of jet in water. Left: vortices detected by Q-criterion. Middle: reconstructed particle tracks (30 snapshots) using tomo-PTV ($ppv = 9 \times 10^{-5}$). Right: Sub-sampled particle tracks ($ppv = 9 \times 10^{-7}$). Tracks are color-coded by velocity magnitude.

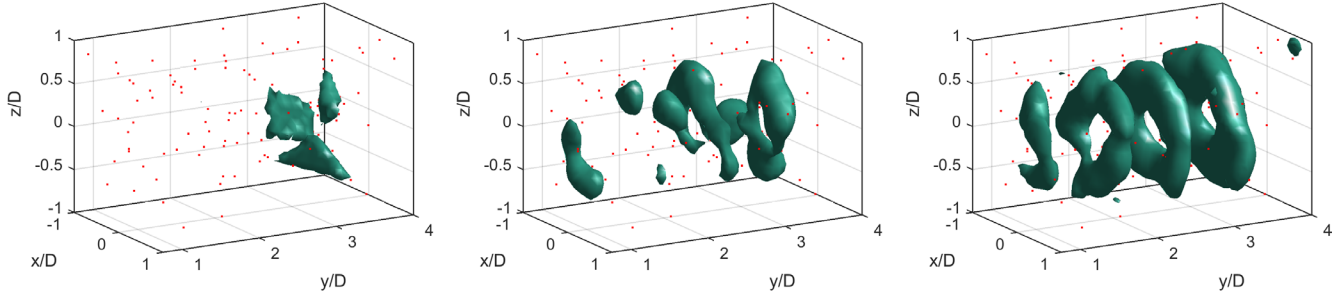


Figure 9 Reconstruction of vortices distribution (isosurface of Q-criterion) from sub-sampled tomo-PTV (95 particle tracks, $ppv = 9.1 \times 10^{-7}$). Left: linear interpolation. Middle: solenoidal filtering. Right: VIC+. Red dots indicate instantaneous position of sub-sampled particles.

A quantitative error assessment makes use of 160 particle tracks in the shear layer selected randomly from the full dataset for benchmark purposes. Here it is assumed that the particle tracks provide a point-wise velocity measurement at significantly higher accuracy than the velocity reconstruction by the methods considered. This is substantiated by the fact that the particle tracks are evaluated over a long trajectory and velocity is found from the analytical derivative of a polynomial fit through the measured particle locations (e.g. Figure 10).

Table 3 lists the RMS error, calculated from the velocity difference between the reconstructed velocity and the benchmark velocity from the above tracks. Results are given for linear interpolation, AGW, solenoidal filtering and VIC+, which uses the velocity material derivative from the particle tracks. For reference, the RMS of velocity difference between the benchmark data and the velocity obtained with cross-correlation analysis of the object (tomo-PIV) is 0.38 vox . When considering the full set of tracers, both solenoidal filtering and VIC+ particle tracks appear to improve (to a similar extent) the measurement accuracy upon tomo-PIV in the shear layer. At lower concentration (ppv) a more marked improvement is observed when employing the particle tracks (VIC+) with respect to divergence free filtering only.

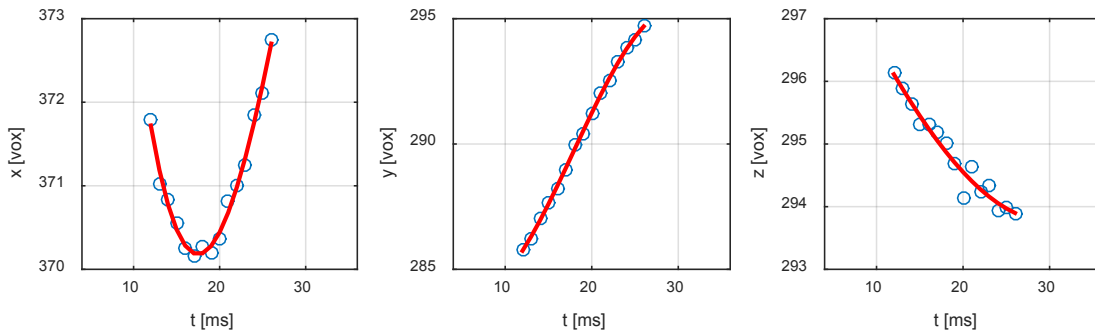


Figure 10 Example of an identified particle track and the 3rd order polynomial fit

Table 3 RMS differences (in voxels) of the reconstructed velocity fields with respect to the instantaneous velocity from 160 benchmark tracks. Points are selected along the jet shear layer.

ppv	# particles	ϵ_{LIN}	ϵ_{AGW}	$\epsilon_{\text{div-free}}$	$\epsilon_{\text{VIC+}}$
9.1×10^{-7}	95	2.5	2.6	2.2	1.8
4.5×10^{-6}	470	1.7	1.9	1.2	1.0
9.0×10^{-6}	940	1.4	1.6	0.9	0.8
4.5×10^{-5}	4700	0.9	1.0	0.4	0.4
9.0×10^{-5}	9400	0.7	0.9	0.3	0.3

5. CONCLUSIONS

A method is proposed to leverage temporal information available by time-resolved tomographic PTV for reconstruction of instantaneous velocity. This improves upon current techniques by not only including penalization of velocity divergence, but also requiring consistency with the temporal derivative of the PTV particle tracks. Hence the procedure is christened as *pouring time into space*. The aim of the proposed technique is to increase spatial resolution and reconstruction accuracy of tomographic PTV in cases where it is limited by the seeding concentration. In addition, reducing requirements on seeding concentration allows for an increase in tomographic PTV measurement volumes in cases where it is limited by the maximum ppp for reconstruction in view of the ghost-particle phenomenon.

An inverse problem is solved to find the velocity field that minimizes a cost function including next to instantaneous velocity, also the velocity material derivative. For regularization, also divergence of vorticity and velocity are included. Velocity and its material derivative are related through the vorticity transport equation and the problem is minimized using the L-BFGS algorithm, where gradients are evaluated efficiently at the computational cost of a single forward computation using an adjoint implementation of the code.

The numerical assessment considers the simulated experiment of a flat-plate turbulent boundary layer from existing DNS data. Increased reconstruction accuracy of the proposed technique over divergence free filtering is found over the full range of seeding concentrations considered. For turbulence statistics, solenoidal filtering is found to require a seeding concentration more than four times larger than the proposed method before it yields a similar reconstruction. The experimental assessment considers the existing tomographic PIV experiment of a jet flow. The data is reprocessed using tomographic PTV. A subset of the particle tracks were considered to simulate lower seeding concentration. When the full set of particle tracks is considered, addition of the temporal information in the reconstruction is not improving the reconstruction, which is ascribed to reconstruction limitations due to measurement errors. When a low seeding concentration is simulated, addition of the velocity material derivative using VIC+ for reconstruction of instantaneous velocity improves the velocity reconstruction and at a seeding concentration of 9×10^{-7} a 20% lower reconstruction error with respect to divergence free filtering only is obtained.

The present study demonstrates that the temporal information available in time-resolved tomographic PTV can be leveraged to improve reconstruction quality of instantaneous velocity on a grid. This allows for reduced seeding concentrations for tomographic PTV at similar reconstruction accuracy, and thereby allowing for increased measurement volumes at the same level of ppp. The experimental assessment considered tomographic PTV, however the technique is equally applicable to other time-resolved volumetric PTV techniques (e.g. 3D-PTV and shake-the-box).

Future work will consider demonstration of the technique in a large-volume tomographic PTV measurement with limited seeding concentration and further development of the code to automatically determine the tuning parameters.

ACKNOWLEDGEMENTS

The authors would like to thank Prof. S. Pirozzoli and Dr. S. Bernardini for providing the DNS dataset and Dr. D. Violato for providing the tomographic PIV dataset used in this study. This research is partly funded by LaVision GmbH.

REFERENCES

- Adrian RJ, Meinhart CD, Tomkins CD (2000) Vortex organization in the outer region of the turbulent boundary layer. *J. Fluid. Mech.* 422:1-54
- Agüí JC, Jiménez J (1987) On the performance of particle tracking. *J. Fluid Mech.* 185:447-468
- Azizli I, Dwight RP, Bijl H (2014) A Bayesian approach to physics-based reconstruction of incompressible flows. In: *Numerical Mathematics and Advanced Applications – ENUMATH 2013, Lausanne*
- Bernardini M, Pirozzoli S (2011) Wall pressure fluctuations beneath supersonic turbulent boundary layers. *Phys. Fluids* 23:085102
- Casa LDC, Krueger PS (2013) Radial basis function interpolation of unstructured, three-dimensional, volumetric particle tracking velocimetry data. *Meas. Sci. Technol.* 24:065304
- Elsinga GE, Scarano F, Wieneke B, van Oudheusden BW (2006) Tomographic particle image velocimetry. *Exp. Fluids* 41:933-947
- Heitz D, Mémin E, Schnörr (2010) Variational fluid flow measurements from image sequences: synopsis and perspectives. *Exp. Fluids* 48:369-393
- Jeon YJ, Chatellier L, David L (2014) Fluid trajectory evaluation based on an ensemble-averaged cross-correlation in time-resolved PIV. *Exp. Fluids* 55:1766
- Keane RD, Adrian RJ, Zhang Y (1995) Super-resolution particle image velocimetry. *Meas. Sci. Technol.* 6:754
- Liu DC, Nocedal J (1989) On the Limited Memory Method for Large Scale Optimization. *Mathematical Programming B*, 45:503-528.
- Lynch KP, Scarano F (2013) A high-order time-accurate interrogation method for time-resolved PIV. *Meas. Sci. Technol.* 24:035305
- Lynch KP, Scarano F (2015) An efficient and accurate approach to MTE-MART for time-resolved tomographic PIV. *Exp. Fluids* 56:66
- Malik NA, Dracos T, Papanoniou DA (1993) Particle tracking velocimetry in three-dimensional flows. *Exp. Fluids* 15:279-294

- Neeteson NJ, Rival DE (2015) Pressure-field extraction on unstructured flow data using a Voronoi tessellation-based networking algorithm: a proof-of-principle study. *Exp. Fluids* 56:44
- Novara M, Batenburg KJ, Scarano F (2010) Motion tracking-enhanced MART for tomographic PIV. *Meas. Sci. Technol.* 21:035401
- Pröbsting S, Scarano F, Bernardini M, Pirozzoli S (2013) On the estimation of wall pressure coherence using time-resolved tomographic PIV. *Exp. Fluids* 54:1567
- Scarano F (2013) Tomographic PIV: principles and practice. *Exp. Fluids* 24:012001
- Scarano F, Moore P (2012) An advection-based model to increase the temporal resolution of PIV time series. *Exp. Fluids* 52:919-933
- Schanz D, Schröder A, Gesemann S, Michaelis D, Wieneke B (2013) 'Shake The Box': A highly efficient and accurate Tomographic Particle Tracking Velocimetry (TOMO-PTV) method using prediction of particle positions. In: 10th Int. Symp. on PIV, Delft, The Netherlands
- Schneiders JFG, Dwight RP, Scarano F (2014) Time-supersampling of 3D-PIV measurements with vortex-in-cell simulation. *Exp. Fluids* 55:1692
- Schroder A, Schanz D, Michaelis D, Cierpka C, Scharnowski S, Kähler CJ (2015) Advances of PIV and 4D-PTV "Shake-The-Box" for Turbulent Flow Analysis –the Flow over Periodic Hills. *Flow Turbulence Combust.*
- Sitou A, Riethmuller ML (2001) Extension of PIV to super resolution using PTV. *Meas. Sci. Technol.* 12:1398
- Vedula P, Adrian R (2005) Optimal solenoidal interpolation of turbulent vector fields: application to PTV and super-resolution PIV *Exp. Fluids* 39, 213-221
- Violato D, Scarano F (2011) Three-dimensional evolution of flow structures in transitional circular and chevron jets. *Phys. Fluids* 23:124104
- Zhong JL, Weng JY, Huang TS (1991) Vector field interpolation in fluid flow. *Digital signal processing* 1991. In: *Int. Conf. on DSP*, Florence, Italy